IEEE Access
Multidisciplinary | Rapid Review | Open Access Journal

Received September 16, 2021, accepted October 31, 2021, date of publication November 8, 2021,
date of current version November 16, 2021.

Digital Object Identifier 10.1109/ACCESS.2021.3126378

Adaptive Switching Frequency Selection Based on Two-Step Efficiency Optimization for Grid-Connected Inverters

AHMED KORAN[1], (Member, IEEE), SAHER ALBATRAN[2], (Senior Member, IEEE), AND DOAA ALSHORMAN[1]

[1]Department of Electrical Power Engineering, Yarmouk University, Irbid 21163, Jordan
[2]Department of Electrical Engineering, Jordan University of Science and Technology, Irbid 22110, Jordan

Corresponding author: Ahmed Koran (akoran@yu.edu.jo)

ABSTRACT A two-step efficiency optimization of a three-phase voltage source inverter with series R damped LCL filter is proposed. The first optimization step aims to find the optimal parameters of the series R damped LCL filter at rated load conditions. The objective function of step-one is to minimize the values of the passive elements of the filter-stage. Afterward, the magnetic cores of inductors are thoroughly designed using soft magnetic powder materials. This design is proposed to specify the smallest core-size required based on the value of the inductance found in step-one of the optimization. The second optimization step aims to optimally select the switching frequency of the inverter-stage considering load variations. This optimization is based on the optimized filter-stage parameters. The proposed objective function of step-two aims to minimize the power losses in the inverter-stage and filter-stage while limiting the harmonic-levels at the point of common coupling. Detailed loss-formulation including filter-stage core and copper losses is thoroughly presented. Teaching-learning-based optimization algorithm is adopted to perform the optimization problem. Experiment and simulation are done to justify the proposed optimization procedure.

INDEX TERMS Voltage source inverter (VSI), passive filters, teaching-learning-based optimization (TLBO), core losses.

I. INTRODUCTION

Inverter output is to be interfaced with the utility-grid through a low-pass filter-stage. This filter-stage is used to ensure that harmonics are within the limits specified by international standards. In high-order filters, the high input-admittance at the resonance frequency may require using either a passive or an active damping technique. Both techniques are used to attenuate the peak value of the input-admittance of the filter at the resonance frequency. If active damping is used, the number of sensors is increased, complicated controllers are needed, and the robustness of the filter may not be ensured [1]–[4]. Conversely, passive damping allows grid-connected VSI to be more robust and more stable. Unfortunately, the cost of the filter will be increased, and more losses will be generated [5]–[9]. Damping resistors are used to reduce the risk of harmonic amplification at the point of common coupling (PCC) and hence minimize interactions between source and load impedances [10]–[12]. Damping resistors are connected in series or parallel with the filter capacitor. The simplest topology in design and implementation is the series R damped LCL filter. This topology is simple in design and implementation, reduces the attenuation, suppresses the peak resonance, but unfortunately, may increases damping power losses.

Achieving high efficiency for grid-connected VSI with series R damped LCL filter is desirable by reducing the power losses of the inverter-stage and the filter-stage and by limiting the harmonic-levels at the PCC. However, this leads to an increase in the cost unless an optimization is performed. A Teaching-learning-based optimization (TLBO) algorithm is utilized in this work to optimally select the values of the filter-stage parameters and the switching frequency in order to maximize the overall efficiency considering load variations.

Inverter-stage power losses are categorized as switching losses (Turn-on and Turn-off), static losses (blocking/conduction), gate driver losses, and diode reverse recovery losses [13]. The significant power losses are due to

The associate editor coordinating the review of this manuscript and approving it for publication was Bijoy Chand Chatterjee.

the turn-on and turn-off of the semiconductor switch, the diode turn-off (reverse recovery), and the conduction losses. Whereas the blocking and gate driver losses are insignificant and are ignored.

The efficiency of the inverter-stage depends on the modulation technique to be utilized. Different pulse-width modulation (PWM) techniques are introduced in literature to enhance inverter's efficiency [14]–[18]. In [14] different PWM methods including sinusoidal PWM (SPWM), space vector PWM (SVPWM), and discontinuous PWM (DPWM) are utilized to model inverter-stage losses. The DPWM reduces the switching losses, inverter size, and cost. The near state pulse-width modulation (NSPWM) was proposed in [15]. The difference between the NSPWM method and the conventional methods is in the ability to reduce the common mode voltage (CMV), common mode current (CMC), and switching losses. In [16], the minimum switching losses PWM (MSLPWM) method, which is basically an SVPWM with special switching sequences, is proposed. This technique leads to reduction in switching losses and harmonic distortion over the conventional SVPWM. The variable switching frequency PWM (VSFPWM) methods is proposed in [17] to reduce switching losses with the same output current quality as the SVPWM method. By reducing the number of commutation without increasing the load, the high power side losses and driving losses are reduced.

Filter-stage power losses include: (i) the magnetization losses due to hysteresis and eddy current; which is known as the core losses, (ii) copper losses, and (iii) damping losses. There are four approaches to formulate the magnetization losses; hysteresis model, empirical equation (improved Steinmetz equation), the loss separation approach, and calculation of the losses with a loss map [19] and [20]. Steinmetz's equation (SE) is an empirical equation that is used to calculate the core losses with sinusoidal excitation. This equation depends on the magnetization frequency and the maximum magnetic flux density. Different version of Steinmetz's equation are reported in literature [21]–[23].

Since the inverter output is non-sinusoidal, the modified Steinmetz equation (MSE) is proposed as an improvement to Steinmetz equation (SE). Modified Steinmetz equation defines the physical origin of the losses and assumes a relationship between the time variation of magnetic flux (B) and core losses [21]. The magnetization frequency in SE is replaced by an equivalent frequency in MSE. However, this method is not self-consistent because of the random definition of the average flux changing rate (dB/dt) and the significant change of Steinmetz coefficient (α) with the equivalent frequency.

The generalized Steinmetz equation (GSE) which is the development formulation of MSE is used for the calculation of core losses with non-sinusoidal waveforms. This method is more accurate than MSE [22]. In most cases, the GSE requires only readily available sinusoidal losses data. This formulation uses the instantaneous flux density and its changing rate to describe the core losses. Improved generalized Steinmetz equation (IGSE) is used to calculate the losses of any flux waveform without requiring additional parameter beyond the parameter of SE. This equation replaces the instantaneous flux density by its peak-to-peak value. Improved generalized Steinmetz equation has a better accuracy for extreme duty cycle cases and switching frequency applicability [23]. However, in some application, where the losses are calculated based on a constant flux, the IGSE is not highly accurate.

Waveform coefficient Steinmetz equation (WCSE) is used to link non-sinusoidal waveform to a sinusoidal waveform. This process is achieved by using a coefficient defined as the ratio between the area of magnetic flux density waveform for non-sinusoidal and sinusoidal. WCSE gives an accuracy more than GSE and IGSE for normal duty cycle range [23]. Regrettably, the equation is not valid for low switching frequency applications.

Improved improved-generalized Steinmetz equation (IIGSE) calculates the core losses caused by magnetic relaxation process [19]. There are four additional parameters to be added to the model compared to the previous models. These parameters should be obtained by measurement, and hence the IIGSE is complicated for practical use. The author of [20] introduced an approach to calculate the core losses under DC bias condition. This approach is called the Steinmetz pre-magnetization graph (SPG) where the graph shows the dependency of the Steinmetz parameters on pre-magnetization.

Filter-stage copper losses are considering the winding of magnetic components including skin and proximity effects. The magnitude of these losses depends on the *ac* and *dc* resistance. Analytical and numerical methods for calculating the winding copper losses are reported in literature [24]–[30]. Analytical methods such as Bessel function method and Dowell's method are presented in [24] and [25]. Finite element (FE) analysis is used to calculate the copper losses in an arbitrary level of accuracy as in [26]. Loss under the condition of non-sinusoidal excitation currents is considered in [27]. The one-dimensional method for calculating the AC resistance of multilayer winding is proposed in [28] and [29]. In [30] the author presented an efficient solution of a FE method to evaluate the copper losses in current carrying conductor.

Based on the previous discussion, the power losses associated with the inverter-stage and the filter-stage are highly dependent on the selection of switching frequency, which will be mathematically introduced in the next section. Accordingly, this selection is vital in improving the total efficiency of the system. In this study, a two-step optimal design methodology to minimize the power losses of the inverter-stage and the filter-stage is proposed. The proposed algorithm adaptively changes the switching frequency of the system considering load variations.

II. INVERTER-STAGE LOSS FORMULATION

Three-phase VSI, which has six IGBTs with antiparallel diodes is utilized in this study and is defined as the

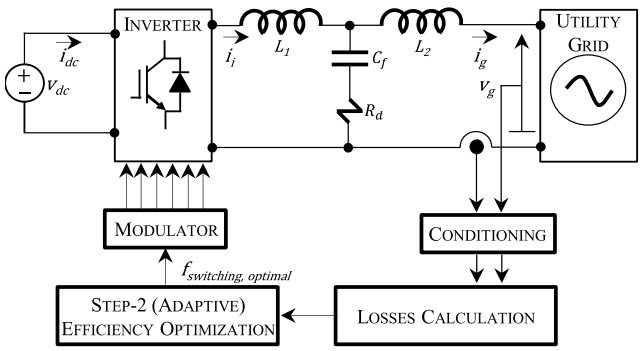

FIGURE 1. Optimization of grid-connected voltage source inverter with series R damped LCL filter.

inverter-stage as in Figure 1. The current flow through the IGBT switches multiplied by the small voltage drop across the switch during the on-state introduces conduction losses. For SPWM, the average conduction losses in the IGBT (P_{C_IGBT}) and the antiparallel diode (P_{C_Diode}) can be given as in (1-2) [31] and [32].

$$P_{C\_IGBT} = \frac{V_{CE0} i_{pk}}{2\pi} + \frac{R_{on} i_{pk}^2}{8} + \left(\frac{V_{CE0} i_{pk}}{8} + \frac{R_{on} i_{pk}^2}{3\pi} \right) m \cos\theta \quad (1)$$

$$P_{C\_Diode} = \frac{V_{f0} i_{pk}}{2\pi} + \frac{R_f i_{pk}^2}{8} + \left(\frac{V_{f0} i_{pk}}{8} + \frac{R_f i_{pk}^2}{3\pi} \right) m \cos\theta \quad (2)$$

where R_{on} and V_{CE0} are the on-state resistance and threshold voltage of IGBT, respectively. Those parameters are found from the voltage-current characteristics curves in manufacturer datasheet. The parameter m is the modulation index, $cos\theta$ is the power factor, R_f and V_{f0} are the on-state forward resistance and threshold voltage of the diode, respectively. i_{pk} is the peak value of the output phase current. The curve fitting method is used to determine the losses in terms of collector current, junction temperature, dc-link voltage, and gate resistance.

The switching losses occur because of the transitions from on-state to off-state and vice versa. Curve fitting method is used to determine the turn-on energy (E_{on}) and the turn-off energy (E_{off}) per pulse. These energy losses are expressed in terms of collector current (i_c), junction temperature (T_j), gate resistance (R_g), and *dc*-link voltage (V_{dc}). The average switching losses in the IGBT (P_{sw_IGBT}) can be expressed in term of switching frequency (f_{sw}) as follow in (3-5) [32].

$$P_{sw\_IGBT} = \frac{E_{on} + E_{off}}{\pi} f_{sw} \quad (3)$$

$$E_{on} = E_{on}(i_c, T_j) * \frac{E_{on}(R_{g,on})}{E_{on}(R_{g.on.test})} * \frac{V_{dc}}{V_{dc,test}} \quad (4)$$

$$E_{off} = E_{off}(i_c, T_j) * \frac{E_{off}(R_{g,off})}{E_{off}(R_{g,off,test})} * \frac{V_{dc}}{V_{dc,test}} \quad (5)$$

where $R_{g,on}$ is the turn-on gate resistance and $R_{g,off}$ is the turn-off gate resistance. The subscript 'test' denotes the parameter value, which is used in the tests for energy losses measurements.

The diode reverse recovery losses occurred because of stored charges in the depletion layer and the p or n layers when the diode transition from the conducting to the non-conducting state. By using curve-fitting method, the reverse recovery energy (E_{rr}) can be expressed in term of diode's forward current (i_f), gate resistance (R_g), *dc*-link voltage (V_{dc}), and junction temperature (T_j) as in (6-7) [32].

$$P_{rr\_diode} = \frac{E_{rr}}{\pi} f_{sw} \quad (6)$$

$$E_{rr} = E_{rr}(i_f, T_j) * \frac{E_{rr}(R_{g,on})}{E_{rr}(R_{g,on,test})} * \frac{V_{dc}}{V_{dc,test}} \quad (7)$$

According to the previous analysis, the total losses of the inverter-stage is formulated as in (8).

$$P_{loss\_total} = 6(P_{C\_IGBT} + P_{C\_diode} + P_{sw\_IGBT} + P_{rr\_diode}) \quad (8)$$

III. FILTER-STAGE LOSS FORMULATION

A. CORE LOSS FORMULATION

The core losses calculation is a vital step to design the LCL-type filter. Several methods of empirical approaches have been developed to calculate core losses of the filter-stage. The Steinmetz equation is the most common method. It is defined with sinusoidal excitations as in (9) [19].

$$P_C = k \cdot f^a \cdot B_m^\beta \quad (9)$$

where k, a, and β are the Steinmetz parameters provided by the manufacturer in the cores-datasheet or through curve fitting. The parameter B_m is the magnitude of the *ac* flux density and f is the excitation frequency. The MSE was developed to calculate the core losses with non-sinusoidal excitations. It expresses the relation between core losses and the time variation of magnetic flux density (dB/dt) as in (10-11) [21].

$$P_C = \left(k \cdot f_{eq}^{a-1} \cdot B_m^\beta \right) \cdot f \quad (10)$$

$$f_{eq} = \frac{2}{\Delta B^2 \pi^2} \int_0^T \left(\frac{dB}{dt} \right)^2 dt \quad (11)$$

where ΔB is the peak-to-peak magnetic flux density, f is the excitation frequency and f_{eq} is the equivalent frequency. The GSE considers both the variation of magnetic flux density and the instantaneous value as well. It can be used to calculate core losses for any flux density waveform as in (12-13) [22].

$$P_c = \frac{k_1}{T} \int_0^T \left| \frac{dB}{dt} \right|^\alpha |B(t)|^{\beta-\alpha} dt \quad (12)$$

$$k_1 = \frac{k}{2^{\beta-\alpha} 2\pi^{\alpha-1} \int_0^{2\pi} |\cos\theta|^\alpha \, d\theta} \quad (13)$$

where $B(t)$ is the instantaneous flux density and T is the period of flux waveform. The impact of magnetization history is considered by using the IGSE. This method replaces the instantaneous magnetic flux density with the peak-to-peak value as in (14-15) [23].

$$P_c = \frac{k_i}{T}\int_0^T \left|\frac{dB}{dt}\right|^{\alpha} |\Delta B|^{\beta-\alpha} dt \tag{14}$$

$$k_i = \frac{k}{2^{\beta-\alpha}\pi^{\alpha-1}\int_0^{2\pi} |\cos\theta|^{\alpha} d\theta} \tag{15}$$

The WCSE is proposed to modify the original SE. The core losses due to non-sinusoidal waveforms can be correlated to the sinusoidal waveforms as in (16) [23].

$$P_C = \lambda \cdot k \cdot f^{a} \cdot B_m^{\beta} \tag{16}$$

where λ is the ratio of the area of magnetic flux waveform for sinusoidal and non-sinusoidal excitation. Core losses due to magnetic relaxation effect are proposed by improved-improved generalized Steinmetz equation. This means that the magnetization change when a constant field is applied, the residual energy loss still occurs as in (17-19) [19].

$$P_C = \frac{1}{T}\int_0^T k_i \left|\frac{dB}{dt}\right|^{\alpha} (\Delta B)^{\beta-\alpha} dt C \sum_{l=1}^{n} Q_{rl} P_{rl} \tag{17}$$

$$P_{rl} = \frac{1}{T} k_r \left|\frac{d}{dt} B(t_-)\right|^{\alpha_r} (\Delta B)^{\beta_r} \left(1 - e^{-\frac{t_1}{\tau}}\right) \tag{18}$$

$$Q_{rl} = e^{-q_r} \left|\frac{dB(t_+)/dt}{dB(t_-)/dt}\right| \tag{19}$$

where $\alpha, \beta, k_i, \alpha_r, \beta_r, k_r, \tau$, and q_r are the material parameters, τ is the relaxation time, t_1 is the duration of the constant flux, $dB(t_+)$, $dB(t_-)$ are the flux density after and before switching, respectively.

In this study, the core losses are calculated based on a new core losses fit formula proposed by Chang Sung Corporation (CSC). The core losses are tested at all frequencies and found that the real core losses and new core losses fit formula results match up very well [33]. The equation of the new core losses fit formula is illustrated as in (20-21).

$$P_c = 0.001 \Delta B^{a} v \left(bf + cf^{d}\right) \tag{20}$$

$$\Delta B = \frac{100 \Delta I L}{N A_e} \tag{21}$$

where P_c is core losses [W], ΔB is flux density [KGauss], v is volume [cc], a, b, c, and d are constants specified in core's datasheets, ΔI is current ripple [A], L is inductance at peak current [μH], N is number of turns, and A_e is core cross section area [cm^2].

B. COPPER LOSS FORMULATION

The winding power losses of filter-stage inductors are comprised of the *dc* losses and *ac* losses. The *dc* losses are caused due to the flow of the *dc* current through the winding while the *ac* losses are a result of skin effect and proximity effect. Both of these effects cause an increase in the winding resistance with the operating frequency. The *Dowell's* equation of round wire windings conducting both *dc* and *ac* under non-sinusoidal condition is adopted. The total winding power losses (P_c) due to the current flow are as in (22) [24].

$$P = I^2 (R_{ac} + R_{dc}) \tag{22}$$

Applying the *Fourier* series of non-sinusoidal current, the following is obtained as in (23-24).

$$i(t) = I_0 + \sum_{j=1}^{\infty} \sqrt{2} I_j \cos(j\omega t) \tag{23}$$

$$I_j = \frac{\sqrt{2}}{j\pi} i_{PK} \sin(j\pi D) \tag{24}$$

where j is the harmonic number, D is the duty cycle, I_0 is the *dc* component and is equal to the multiplication of D and i_{pk}, I_j is the harmonic rms value.

The round wire winding *dc* resistance is given as in (25).

$$R_{dc} = \frac{4 l_T m N}{\pi \sigma d^2} \tag{25}$$

where l_T is the mean turn length, m is the number of layer, N is the number of turns in one layer, σ is the material conductivity, d is the diameter of the bare round wire. The loss due to an individual Fourier component is expressed as in (26-27).

$$P_{dc} = I_0^2 R_{dc} \tag{26}$$

$$P_j = I_j^2 R_{dc} \sqrt{j\varphi} \left[\frac{\sinh 2\sqrt{j\varphi} + \sin 2\sqrt{j\varphi}}{\cosh 2\sqrt{j\varphi} - \cos 2\sqrt{j\varphi}} + \frac{2(M^2-1)}{3} \frac{\sinh\sqrt{j\varphi} + \sin\sqrt{j\varphi}}{\cosh\sqrt{j\varphi} - \cos\sqrt{j\varphi}}\right] \tag{27}$$

where φ is defined as $d/\delta\sqrt{\eta\pi/4}$, δ is the skin depth given by $1/\sqrt{\pi\mu\sigma f}$, η is the porosity factor, μ is the permeability, σ is the conductivity.

The total winding copper losses is defined as in (28).

$$P_{cu} = I_0^2 R_{dc} + F_H F_R I_1^2 R_{dc} \tag{28}$$

where F_H and F_R are defined in (29-30) and are the harmonic loss factor and resistance factor, respectively.

$$F_H = \frac{\sum_{j=1}^{\infty} P_j}{P_1} \tag{29}$$

$$F_R = \frac{R_{ac}}{R_{dc}} = \sqrt{j\varphi}\left[\frac{\sinh 2\sqrt{j\varphi} + \sin 2\sqrt{j\varphi}}{\cosh 2\sqrt{j\varphi} - \cos 2\sqrt{j\varphi}} + \frac{2(M^2-1)}{3} \frac{\sinh\sqrt{j\varphi} + \sin\sqrt{j\varphi}}{\cosh\sqrt{j\varphi} - \cos\sqrt{j\varphi}}\right] \tag{30}$$

The resistance factor is affected by increasing the number of layers but it is not affected by increasing the number of turns per layer as shown in (30). The number of turns affects the *dc* and *ac* resistance. The previous equations compute the

power losses of each individual harmonic and are summoned together to find the total winding copper losses in multiple-layers. The copper losses in this study are calculated based on a formula proposed by CSC. These losses depend on the rated current and the resistance of the wire. Increasing the number of turns leads to an increase in the wire loss [33]. The equation of copper losses are illustrated as in (31-33) [34].

$$P_{cu} = 0.001 I_{rms}^2 R_{DC} \tag{31}$$

$$R_{DC} = R_{DC}^{(20)}(1 + (3.93 * 10^{-3} * (T_{wire} - 20))) \tag{32}$$

$$R_{DC}^{(20)} = \frac{0.001 * 1.7 l_w N}{0.01 A_e} \tag{33}$$

where P_{cu} is copper losses [W], I_{rms} is the rms rated current [A], R_{dc} is the *dc* resistance at the required temperature [mΩ], $R_{DC}^{(20)}$ is the *dc* resistor at 20° [mΩ], T_{wire} is temperature of wire [C°], and l_w is the wire length [cm].

IV. TWO-STEP EFFICIENCY OPTIMIZATION: RESULTS AND DISCUSSION

In this section, the TLBO algorithm is utilized to optimally design a grid-connected three-phase VSI alongside series R damped LCL filter. The optimization is carried on two-steps: (i) optimal selection of filter-stage parameters is performed in order to minimize the total values of filter-inductance and filter-capacitance. The optimization is executed at the rated load conditions. (ii) Based on the selected filter-stage parameters, step-two of the optimization is executed to optimally select the inverter-stage switching frequency taking into consideration load variations. The proposed objective function minimizes overall losses including filter-stage and inverter-stage losses, and hence, maximizes system efficiency.

TLBO is a population-based metaheuristics search (MS) algorithm introduce in 2011. The algorithm mimics the traditional teaching-learning phenomenon of a classroom. Additionally, the algorithm has simple concept, easy implementation, rapid convergence, and requires few specific controlling parameters like population size and number of generations [35]. It has been applied to handle constrained, multi-objective, and dynamic optimization problems as well [36].

A. STEP-ONE: PARAMETERS OPTIMIZATION OF SERIES R DAMPED LCL FILTER

The parameters of the series R damped LCL filter (L_1, L_2, C_f, R_d) are selected in order to minimize the value of the total inductances and the filter-capacitance as in (34) [10] and [37]. A weighting factor (w) is considered as a trade-off between minimizing the values of the total inductance and the capacitance.

$$F_{obj} = w \times (L_1 + L_2) + (1 - w) \times C_f \tag{34}$$

To solve this optimization problem, TLBO algorithm is used. The number of iterations is selected to be 100 and the number of population is 20. The constraints of the objective function are defined as the lower and upper limits of filter parameters alongside total harmonic distortion (THD) and total demand distortion (TDD) based on IEEE-519 standard. The THD is defined as "the ratio of the root-mean-square of the harmonic content to the root-mean-square value of the fundamental quantity, expressed as a percent of the fundamental" [36]. While the TDD is defined as "the ratio of the root mean square of the harmonic content, expressed as a percent of the maximum demand current" [38]. The minimization problem is formulated as in (35)

$$\begin{aligned}
&\textbf{Min} \quad F_{obj} = w \times (L_1 + L_2) + (1 - w) \times C_f \\
&\text{Subjected to :} \quad \left.\begin{array}{c} TDD \le 5.0 \\ max(I_H) \le 4.0 I_{max} \; \forall H < 11 \\ max\,(I_H) \le 2.0 I_{max} 11 \le \forall H < 17 \\ max\,(I_H) \le 1.5 I_{max} 17 \le \forall H < 23 \\ max(I_H) \le 0.6 I_{max} 23 \le \forall H < 35 \\ max\,(I_H) \le 0.3 I_{max} 35 \le \forall H \end{array}\right\} \\
&R_d^{min} \le R_d \le R_d^{max} \\
&L_1^{min} \le L_1 \le L_1^{max} \\
&L_2^{min} \le L_2 \le L_2^{max} \\
&C_f^{min} \le C_f \le C_f^{max}
\end{aligned} \tag{35}$$

where w refers to the weighting factor, which is varied from 0.2 to 0.8, R_d^{min} and R_d^{max} are the least and most allowable damping resistors, respectively, L_1^{min} and L_1^{max} are the least and most allowable inverter-side inductance, respectively, L_2^{min} and L_2^{max} are the least and most allowable grid-side inductance, respectively, and C_f^{min} and C_f^{max} are the least and most filter-capacitance, respectively.

The input *dc* voltage is selected 200 V and the current-ripple is chosen as 15% of rated current due to the trade-off among inductor size, IGBT switching and conduction losses, and copper and core losses [6]. Table 1 shows the optimal values of the optimization problem defined in (35) at different weighting factors from 0.2 to 0.8. The weighting factor of 0.2 has a large value of inverter-side inductance with zero grid-side inductance and zero damping resistor. Based on the selected weighting factor, an LC-type filter is suitable for grid connection. Moreover, decreasing the weighting factor would increase the total inductances and reduce the filter-capacitance, which leads to a large filter size and cost. Figure 2 illustrates the frequency response (grid-current to inverter-voltage) of the output filter, which is presented in Table 1 at different weighting factors. It is clear that at a weighting factor of 0.2, the resonance frequency is at 12 MHz and the resonance peak reaches −40 dB, this is justified as the damping resistance is zero based on optimization results of step-one. However, at other weighting factors from 0.3 to 0.8, the resonance peaks vary from −60 dB to −74 dB over a range of frequencies between 2.0 to 3.0 kHz. Briefly, the lower the weighting factor the higher the resonance frequency, and hence a faster controller response to be achieved [39]. In addition, the diagrams show that the gain at the resonance peak is suppressed with the addition of a damping resistor.

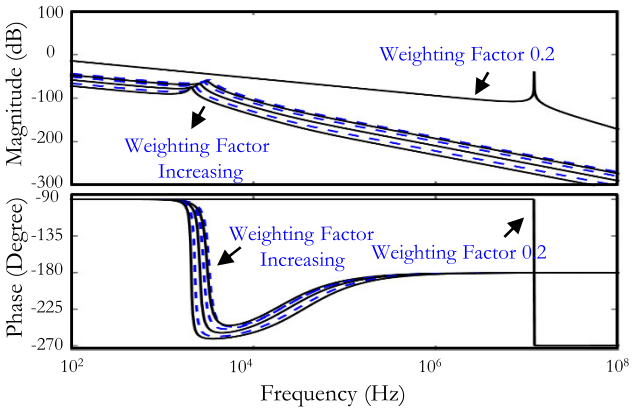

FIGURE 2. Filter frequency response of the series R damped LCL filter at different weighting factors.

TABLE 1. Optimal design results of step-one optimization at different weighting factors.

Weighting Factor	L_1(mH)	L_2(mH)	C_f(μF)	R_d(Ω)
0.2	8.5	0	1.74	0
0.3	2.7	1.6	0.89	8.72
0.4	2.2	1.4	1.21	7.28
0.5	2.2	1.2	1.44	5.44
0.6	2.2	0.92	1.74	3.84
0.7	2.2	0.68	2.23	2.41
0.8	2.2	0.53	2.68	1.66

B. CORE DESIGN AND SELECTION PROCEDURE

In this part, the selection and design of the inductor's cores are presented based on the results of step-one of the proposed optimization procedure. The most utilized magnetic materials that are of industrial interest are the soft magnetic materials. The soft magnetic materials can be easily magnetized and demagnetized [40]. In addition, the soft magnetic materials have low coercivity, high permeability, and low core losses [41]. The inductor's cores considered in this work are made out of magnetic powder and have a toroidal shape-like. Practically, different companies produce powder cores such as; Allied Components, Magnetics Corporation, Amveco Magnetics, Ferronics Incorporation, Flex-Core, and Chang Sung Corporation. Each of these companies has its own design of magnetic cores and magnetic components including inductors, transformers, and filters.

In this work, the magnetic cores manufactured by CSC are chosen to design the cores of inverter-side and grid-side inductors. CSC manufactures different types of soft magnetic powder cores including ferrite and metal cores. The metal cores are either strip or powder. The powder cores include the Moly Permalloy powder (MPP), High Flux, Sendust, Mega Flux, HS, KS, KH, Fine Flux, and HP. The first four types of the powder cores are mainly used for inductors and transformers requiring low losses and inductance stability. Those cores are made of metal alloy powders consisting of nickel, iron, molybdenum, aluminum, and silicon [33]. CSC core-design software assists in selecting the optimum powder core for inverter-based applications.

TABLE 2. Core material design for 8.5 mH.

Material	L (mH)	# OF TURN	μ	Core Losses (W)		Total Losses (W)	
				DC	AC	DC	AC
MPP (CM)	8.52	404	26	0.1	0.3	**13.4**	**13.7**
High Flux (CH)	8.50	239	60	0.2	0.9	**8.1**	**8.8**
Sendust (CS)	8.51	361	60	0.1	0.6	**12.2**	**12.7**
Mega Flux (CK)	8.52	244	75	0.6	2.8	**8.7**	**10.9**
HS (HS)	8.53	260	75	0.2	1	**8.8**	**9.6**
KS (KS)	8.50	311	60	0.3	1.3	**10.6**	**11.6**
KH (KH)	8.51	239	60	0.4	2	**8.3**	**9.9**
Fine Flux (CF)	8.51	317	40	0.1	0.7	**10.6**	**11.2**
HP (HP)	8.54	344	26	0.1	0.4	**11.5**	**11.8**

TABLE 3. Core material design for 2.7 mH.

Material	L (mH)	# OF TURN	μ	Core Losses (W)		Total Losses (W)	
				DC	AC	DC	AC
MPP (CM)	2.71	174	60	0	0.2	**4.7**	**4.8**
High Flux (CH)	2.71	152	125	0.1	0.4	**3.4**	**3.7**
Sendust (CS)	2.71	187	75	0	0.2	**5.1**	**5.3**
Mega Flux (CK)	2.71	123	90	0.3	1.2	**3.6**	**4.5**
HS (HS)	2.70	175	75	0.1	0.4	**3.9**	**4.2**
KS (KS)	2.71	213	60	0.1	0.5	**4.8**	**5.1**
KH (KH)	2.71	168	60	0.1	0.7	**3.8**	**4.4**
Fine Flux (CF)	2.71	150	60	0.1	0.3	**4.1**	**4.3**
HP (HP)	2.70	243	26	0	0.1	**5.4**	**5.5**

TABLE 4. Core material design for 2.2 mH.

Material	L (mH)	# OF TURN	μ	Core Losses (W)		Total Losses (W)	
				DC	AC	DC	AC
MPP (CM)	2.21	240	26	0	0.1	**5.3**	**5.3**
High Flux (CH)	2.21	178	60	0	0.2	**3.3**	**3.5**
Sendust (CS)	2.20	238	60	0	0.1	**5.3**	**5.4**
Mega Flux (CK)	2.20	182	75	0.2	0.7	**3.5**	**4**
HS (HS)	2.20	149	75	0.1	0.3	**3.1**	**3.4**
KS (KS)	2.20	282	40	0.1	0.3	**4.8**	**5.1**
KH (KH)	2.20	177	60	0.1	0.5	**3.4**	**3.7**
Fine Flux (CF)	2.20	287	40	0	0.1	**4.9**	**5**
HP (HP)	2.21	215	26	0	0.1	**4.8**	**4.8**

Based on the optimized results from step-one of the proposed optimization procedure (Table 1), the inverter-side and grid-side inductors are designed according to the CSC design tool. All types of soft magnetic powder cores in CSC are selected for the sake of comparison. Design results are reported in Tables 2-10. Through comparing the different

TABLE 5. Core material design for 1.6 mH.

Material	L (mH)	# OF TURN	μ	Core Losses (W)		Total Losses (W)	
				DC	AC	DC	AC
MPP (CM)	1.60	273	26	0	0.1	**4.6**	**4.7**
High Flux (CH)	1.60	110	125	0.1	0.2	**2.2**	**2.4**
Sendust (CS)	1.60	168	75	0	0.2	**3.7**	**3.8**
Mega Flux (CK)	1.61	124	75	0.1	0.6	**2.6**	**3**
HS (HS)	1.61	129	75	0	0.2	**2.6**	**2.8**
KS (KS)	1.60	177	60	0.1	0.3	**3.3**	**3.5**
KH (KH)	1.60	124	90	0.1	0.3	**2.5**	**2.8**
Fine Flux (CF)	1.60	182	60	0	0.1	**3.4**	**3.5**
HP (HP)	1.60	239	26	0	0.1	**4.1**	**4.1**

TABLE 6. Core material design for 1.4 mH.

Material	L (mH)	# OF TURN	μ	Core Losses (W)		Total Losses (W)	
				DC	AC	DC	AC
MPP (CM)	1.40	142	60	0	0.1	**3**	**3**
High Flux (CH)	1.41	149	60	0	0.1	**2.6**	**2.7**
Sendust (CS)	1.40	152	60	0	0.1	**3.2**	**3.3**
Mega Flux (CK)	1.40	152	75	0.1	0.4	**2.7**	**3**
HS (HS)	1.41	115	75	0	0.2	**2.3**	**2.5**
KS (KS)	1.40	168	60	0.1	0.2	**3.1**	**3.3**
KH (KH)	1.40	148	60	0.1	0.3	**2.6**	**2.8**
Fine Flux (CF)	1.40	173	60	0	0.1	**3.1**	**3.2**
HP (HP)	1.40	190	26	0	0.1	**3.5**	**3.6**

TABLE 7. Core material design for 1.2 mH.

Material	L (mH)	# OF TURN	μ	Core Losses (W)		Total Losses (W)	
				DC	AC	DC	AC
MPP (CM)	1.20	173	60	0	0.1	**3.2**	**3.2**
High Flux (CH)	1.20	128	125	0	0.1	**2.2**	**2.3**
Sendust (CS)	1.20	175	60	0	0.1	**3.2**	**3.3**
Mega Flux (CK)	1.21	134	75	0.1	0.4	**2.4**	**2.7**
HS (HS)	1.20	140	75	0	0.2	**2.4**	**2.5**
KS (KS)	1.21	125	60	0	0.2	**2.5**	**2.7**
KH (KH)	1.201	95	90	0.1	0.3	**2**	**2.2**
Fine Flux (CF)	1.20	124	60	0	0.1	**2.5**	**2.6**
HP (HP)	1.21	176	26	0	0.1	**3.2**	**3.2**

inductor designs using the same magnetic material, a decrease in the inductance value leads to a decrease in the magnetic core size. Accordingly, a decrease in the total losses and the cost of the filter are achieved. When comparing different magnetic core materials for the same inductance value, the higher the inductance value the higher the required number of turns. According to Table 2, it is clear that an increase in the number of turns leads to an increase in permeability, and this leads to an increase in the wire losses and a decrease in core losses. Thus, increasing the wire losses results in an increase in the cost. In addition, the Mega flux material has achieved the maximum value of core losses when compared with the other materials. Furthermore, the MPP material has given the minimum value for core losses and the maximum values for the wire losses and number of turns.

TABLE 8. Core material design for 0.915 mH.

Material	L (mH)	# OF TURN	μ	Core Losses (W)		Total Losses (W)	
				DC	AC	DC	AC
MPP (CM)	0.917	109	60	0	0.1	**2.2**	**2.2**
High Flux (CH)	0.918	124	60	0	0.1	**1.9**	**2**
Sendust (CS)	0.920	118	75	0	0.1	**2.4**	**2.4**
Mega Flux (CK)	0.919	126	75	0.1	0.3	**2**	**2.2**
HS (HS)	0.916	111	75	0	0.1	**1.9**	**2**
KS (KS)	0.921	136	60	0	0.2	**2.3**	**2.5**
KH (KH)	0.918	124	60	0	0.2	**2**	**2.1**
Fine Flux (CF)	0.920	137	60	0	0.1	**2.3**	**2.4**
HP (HP)	0.928	130	26	0	0.1	**2.6**	**2.6**

TABLE 9. Core material design for 0.675 mH.

Material	L (mH)	# OF TURN	μ	Core Losses (W)		Total Losses (W)	
				DC	AC	DC	AC
MPP (CM)	0.677	119	60	0	0	**2**	**2.1**
High Flux (CH)	0.675	104	125	0	0.1	**1.5**	**1.6**
Sendust (CS)	0.678	128	60	0	0.1	**2.2**	**2.2**
Mega Flux (CK)	0.675	114	75	0.1	0.2	**1.6**	**1.8**
HS (HS)	0.680	120	75	0	0.1	**1.7**	**1.7**
KS (KS)	0.676	124	60	0	0.1	**1.9**	**2**
KH (KH)	0.677	113	60	0	0.2	**1.6**	**1.7**
Fine Flux (CF)	0.677	125	60	0	0.1	**1.9**	**2**
HP (HP)	0.683	136	26	0	0	**2.3**	**2.3**

Figure 3 shows the relationship between both the core and copper losses in respect to the number of turns as listed in Table 2 of 8.5 mH inductance. The more turns required the higher are the core and copper losses. However, the curve shows that increasing the number of turns will increase the copper losses and decrease the core losses. This is due to increased wires-length.

C. STEP-TWO: OPTIMAL SWITCHING FREQUENCY CONSIDERING LOAD VARIATIONS

Step-two of the proposed optimization algorithm is to optimally select the switching frequency of the inverter-stage

TABLE 10. Core material design for 0.534 mH.

Material	L (mH)	# OF TURN	μ	Core Losses (W)		Total Losses (W)	
				DC	AC	DC	AC
MPP (CM)	0.535	119	60	0	0	**1.8**	**1.9**
High Flux (CH)	0.539	82	125	0	0.1	**1.2**	**1.2**
Sendust (CS)	0.538	126	60	0	0	**1.9**	**2**
Mega Flux (CK)	0.538	96	75	0	0.2	**1.4**	**1.5**
HS (HS)	0.537	98	75	0	0.1	**1.4**	**1.4**
KS (KS)	0.536	119	60	0	0.1	**1.7**	**1.7**
KH (KH)	0.535	92	90	0	0.1	**1.3**	**1.4**
Fine Flux (CF)	0.537	120	60	0	0	**1.7**	**1.7**
HP (HP)	0.538	112	60	0	0	**1.7**	**1.7**

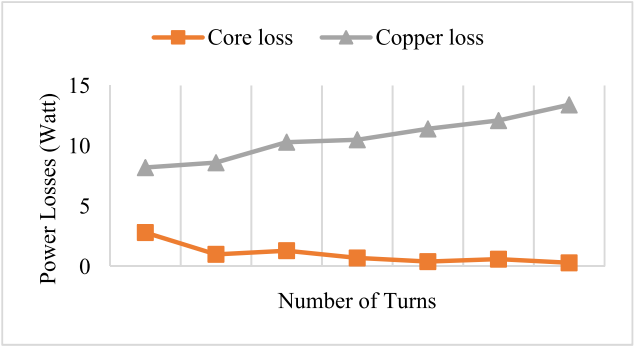

FIGURE 3. The relationship between inductor number of turns and power losses for L = 8.5 mH.

considering load variations. Inputs to step-two are the optimized filter-stage parameters based on step-one of the optimization procedure. The mathematical formulation of the objective function is described as in (36). Figure 4 illustrates a detailed flowchart of the proposed optimization procedure.

$$
\begin{aligned}
&\boldsymbol{min\ P_{Loss} = \left(6(P_{C\_IGBT} + P_{C\_diode} + P_{sw\_IGBT} + P_{rr\_diode})\right) + P_C + P_{cu}}\\
&\boldsymbol{T_{J,IGBT} \le T_{J,IGBT_{max}}}\\
&\boldsymbol{T_{J,diode} \le T_{J,diode_{max}}}\\
&\boldsymbol{TDD \le TDD_{max}}\\
&\boldsymbol{THD_V \le THD_{V,max}}\\
&\boldsymbol{f_{sw} \ge Kf_{res}}\\
&\boldsymbol{H_{minImax}(\omega) \le H_{Imax}(\omega) \le H_{maxImax}(\omega)}\\
&\boldsymbol{L_1 \le L_{1,max}}\\
&\boldsymbol{L_2 \le L_{2,max}}\\
&\boldsymbol{C_f \le C_{f,max}}\\
&\boldsymbol{R_{dmin} \le R_d \le R_{dmax}}
\end{aligned}
\tag{36}
$$

where TDD is the total demand distortion of the inverter's output current, TDD_{max} is maximum allowed total demand distortion, THD_V is the total harmonic distortion of the

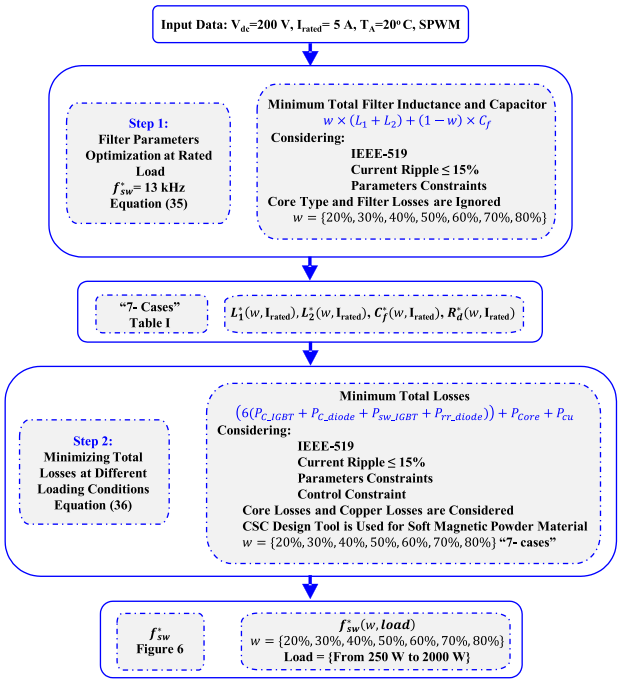

FIGURE 4. Detailed flowchart of the proposed optimization procedure.

inverter's output voltage, THD_{Vmax} is maximum allowed total harmonic voltage distortion, $\boldsymbol{k}$ is constant design factor, $\boldsymbol{f_{sw}}$ is switching frequency in kHz, $\boldsymbol{f_{res}}$ is cutoff frequency of the filter in kHz, $\boldsymbol{H_{minImax}(\omega)}$ is minimum allowed filter gain at maximum load, and $\boldsymbol{H_{maxImax}(\omega)}$ is maximum allowed filter gain at maximum load.

The results obtained solving the problem using TLBO algorithm are summarized in Figure 5. The total power losses and the optimal switching frequency are shown for sundust material considering variable load at different weighting factors. Sundust material is chosen because it is the most cost-effective design material [34]. However, the results show that the weighting factor of 0.2 achieves the minimum total power loss and switching frequency among the other weighting factors at the same load. This is justified as the values of grid-side inductance and a damping resistor are zeros. For higher weighting factors, the value of the filter parameters decrease leading to a decrease in the total power losses and switching frequency of the overall system. In addition, Figure 5 shows that the minimum value of total power losses is achieved at lighter load; the algorithm increases the switching frequency to enhance the quality of the output current. At heavier load conditions, the total power losses are higher; thus, the algorithm reduces the switching frequency while keeping the total demand distortion below 5%.

Figure 6 presents the efficiency of the overall system with variable load condition. A weighting factor of 0.2 has the lowest total power losses as discussed previously hence improving overall efficiency at all load conditions. Moreover, the system efficiency increases with the increase of the output power at the same weighting factor. The peak efficiency is

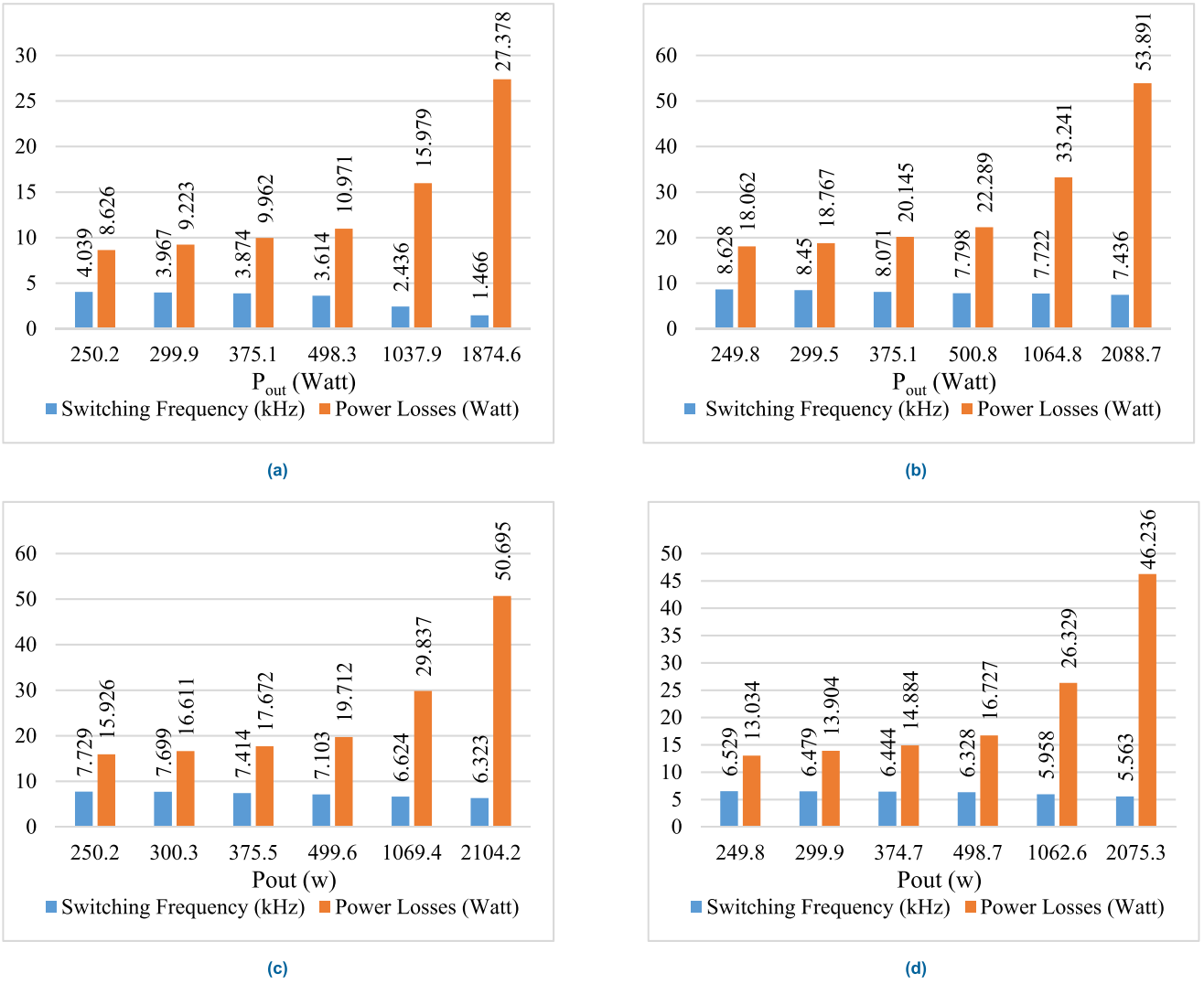

FIGURE 5. The optimal values of switching frequency for variable load and different weighting factors; a) $w = 0.2$, b) $w = 0.4$, c) $w = 0.6$, and d) $w = 0.8$.

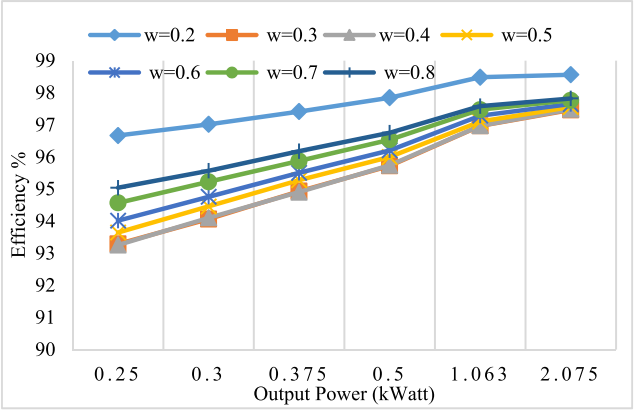

FIGURE 6. Analytical estimated overall efficiency with variable load at different weighting factors.

reported as 98.5%, 97.4%, 97.4%, 97.5%, 97.6%, 97.7%, 97.8% for w = 0.2 to w = 0.8, respectively. The reason of efficiency increase is due to the reduction of filter parameters values and the decrease of switching frequency which in turn decreases the overall power losses.

D. GRID-SIDE HARMONIC ANALYSIS

The current harmonics should be limited at the PCC according to IEEE-519 international standard. The IEEE-519 is defined as: "Recommended Practices and Requirements for Harmonic Control in Electrical Power Systems" [38]. Recommended practice is to be used as a guidance in the design of electrical systems that include both linear and non-linear loads assuming steady-state operation [42]. The limits in this recommended practice are intended for application at the PCC between the system owner or operator and the user. The THD of the current should be limited to less than 5%, measured at the rated output of the VSI.

To evaluate the effectiveness of the optimized design of the LCL-type filter, it is important to measure the output current

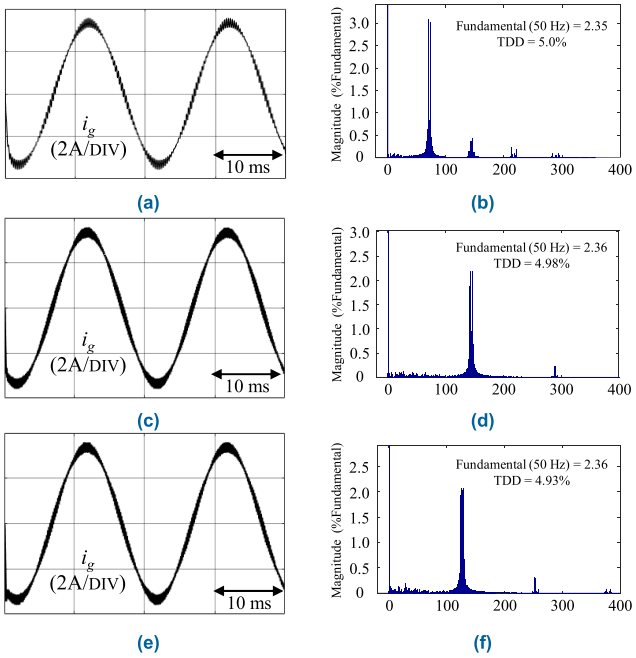

FIGURE 7. Simulated grid current and harmonic content spectrum at different weighting factors, optimal switching frequency, and 0.5 kWatt; (a) and (b) w of 0.2, (c) and (d) w of 0.5 (e) and (f) w of 0.8.

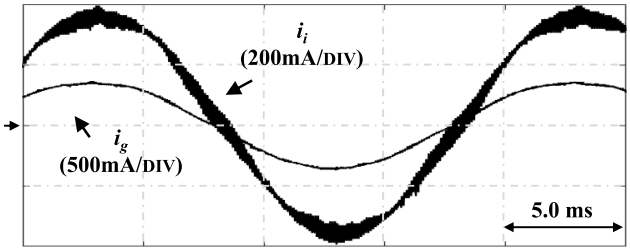

FIGURE 8. Measured inverter-side (i_i) and grid-side (i_g) currents at 0.3 weighting factor and 0.5 kW load. Tektronix current probe (Model: A622) with 100mV/A gain. $L_1 = 2.7$ mH, $L_2 = 1.6$ mH, $C_f = 0.89$ μF, and $R_d = 8.72$ Ω.

harmonics passing through grid-side inductance. In time-domain analysis, grid current is extracted to perform Fast Fourier Transform (FFT) analysis. Figure 7 shows phase 'a' simulated grid-side current waveforms and the corresponding harmonic current spectrums at different weighting factors under steady-state conditions and optimal switching frequency. In Figure 7(a), for 0.2 weighting factor, the optimized filter has a zero grid-inductance and zero damping resistor, this results in higher distortion as compared to the other cases. For 0.8 weighting factor, the THD is 4.93% which is at the high side of distortion compared with other weighting factors. This is due to low value of inductance. Furthermore, it is found that the optimal results of the proposed objective function are reducing the TDD of the grid-side current.

V. EXPERIMENTAL RESULTS

To justify the effectiveness of the two-step efficiency optimization and the core-material selection and design, a prototype is experimentally tested at different weighting factors.

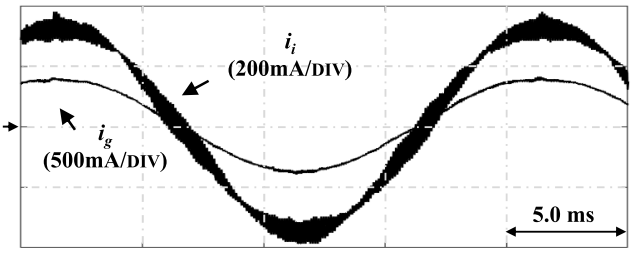

FIGURE 9. Measured inverter-side (i_i) and grid-side (i_g) currents at 0.8 weighting factor and 0.5 kW load. Tektronix current probe (Model: A622) with 100mV/A gain. $L_1 = 2.2$ mH, $L_2 = 0.53$ mH, $C_f = 2.68$ μF, and $R_d = 1.66$ Ω.

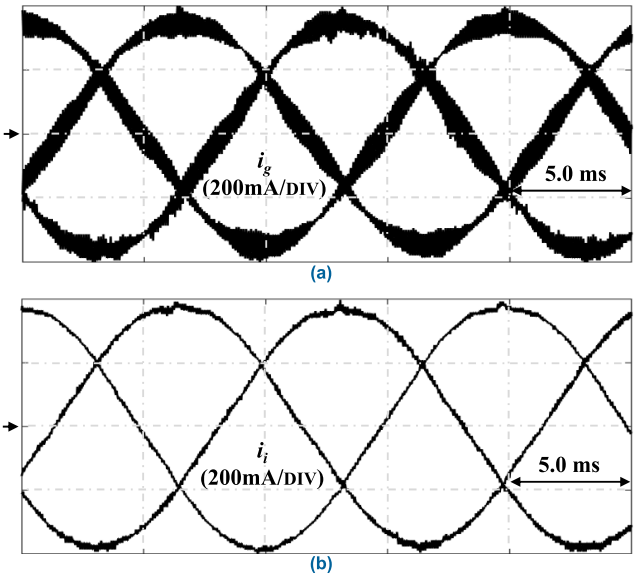

FIGURE 10. Measured three-phase (a) inverter-side (i_i) currents and (b) grid-side (i_g) currents at 0.8 weighting factor and 0.5 kW load. Tektronix current probe (Model: A622) with 100mV/A gain. $L_1 = 2.2$ mH, $L_2 = 0.53$ mH, $C_f = 2.68$ μF, and $R_d = 1.66$ Ω.

A field programmable gate array (FPGA) controller (Model: Terasic DE2-115) is utilized to control the inverter-stage. The *dc*-link voltage is kept constant at 200 V. Figure 8 shows the inverter-side and grid-side currents at 0.3 weighting factor and 0.5 kW output power. Sundust core material is adopted in the experiment as it is cost effective [34]. Inverter-side (L_1) and grid-side (L_2) inductances detailed designs are reported in Table 3 and Table 5. System operating switching frequency based on the two-step optimization problem is 7.91 kHz. The measured THD of the inverter-side current is 4.94% and the measured THD of the grid-side current is 2.41%. The measured system efficiency is 95.29%. Figure 9 illustrates the inverter-side and gird-side currents at 0.8 weighting factor and 0.5 kW output power. Inverter-side (L_1) and grid-side (L_2) inductances detailed designs are reported in Table 4 and 10. The optimal switching frequency based on the two-step optimization problem is 6.33 kHz. The measured THD of the inverter-side current is 5.08% and the measured THD of the grid-side current is 3.06%. The measured system efficiency is 96.35%.

The two sets of experiments prove that the optimized system meets IEEE-519 for maximum harmonic current distortion at the grid and load side. As this work is directed toward improving the system efficiency and reduce heat stress, the proposed work scheme can ensure better thermal response by adjusting the switching frequency to the optimal operating point. This can't be achieved without slightly increasing the THD at the grid side without violating the standards. Furthermore, the experimental results match the analytical estimated efficiency and THD reported in Figure 5 and 7 fairly. Moreover, Figure 10 demonstrates three-phase inverter-side currents (Figure 10(a)) and three-phase grid-side currents (Figure 10(b)) at 0.8 weighting factor and 0.5 kW output power.

VI. CONCLUSION

A two-step optimization problem is formulated to optimally design the parameters of the filter-stage (step-one) and to optimally select the switching frequency of the inverter-stage considering load variations (step-two). The TLBO algorithm is utilized in step-one optimization to minimize the size of the grid-side inductance, inverter-side inductance, and filter-capacitance. In step-two, the losses in the inverter-stage and filter-stage are minimized based on the derived models. This optimization assures the highest efficiency while simultaneously meeting the standard grid-connection requirement. The results obtained can be concluded as follows:

The large value of the inductance is offset by the small value of the capacitance to meet the attenuation requirement. The large value of the capacitance leads to an increase in the low-frequency harmonic content and THD of the grid current.

The decrease in the value of inductance leads to a decrease in the volume of the filter and hence, a reduce of the total losses.

The increase in the value of inductance leads to an increase in the number of turns, which in turn increases the wire copper losses and decreases the core losses.

Mega flux material has the maximum value of core losses while the MPP material has the minimum value of core losses.

MPP material has the maximum values of the wire copper losses and number of turns.

The weighting factor of 0.2 has the minimum switching frequency and the minimum total power losses and hence it has the highest efficiency of 98.5% as compared to other weighting factors.

High weighting factors result in a low value of filter parameters lowering the power losses and switching frequency and hence improving the efficiency.

The lighter loads have the minimum value of power losses, the optimization algorithm increases the switching frequency to enhance the quality of output power.

The heavier loads have the maximum value of power losses, the optimization algorithm reduces the switching frequency to keep the TDD below 5%.

REFERENCES

[1] R. N. Beres, X. Wang, F. Blaabjerg, M. Liserre, and C. L. Bak, "Optimal design of high-order passive-damped filters for grid-connected applications," *IEEE Trans. Power Electron.*, vol. 31, no. 4, pp. 2083–2098, Mar. 2016.

[2] G. Hu, C. Chen, and D. Shanxu, "New active damping strategy for LCL-filter-based grid-connected inverters with harmonics compensation," *J. Power Electron.*, vol. 13, no. 2, pp. 287–295, Mar. 2013.

[3] L. F. J. Meloni, F. L. Tofoli, A. J. J. Rezek, and E. R. Ribeiro, "Modeling and experimental validation of a single-phase series active power filter for harmonic voltage reduction," *IEEE Access*, vol. 7, pp. 151971–151984, 2019.

[4] Q. Zhang, Y. Tang, L. Hou, F. Deng, S. An, and X. Sun, "An active high frequency damping scheme for the current control of L filter-based grid-connected inverter," *IEEE Access*, vol. 7, pp. 171738–171751, 2019.

[5] R. Peña-Alzola, M. Liserre, F. Blaabjerg, R. Sebastián, J. Dannehl, and F. W. Fuchs, "Analysis of the passive damping losses in LCL-filter-based grid converters," *IEEE Trans. Power Electron.*, vol. 28, no. 6, pp. 2642–2646, Jun. 2013.

[6] R. N. Beres, X. Wang, M. Liserre, F. Blaabjerg, and C. L. Bak, "A review of passive power filters for three-phase grid-connected voltage-source converters," *IEEE Trans. J. Emerg. Sel. Topics Power Electron.*, vol. 4, no. 1, pp. 54–69, Mar. 2016.

[7] B. Alamri and Y. M. Alharbi, "A framework for optimum determination of LCL-filter parameters for N-level voltage source inverters using heuristic approach," *IEEE Access*, vol. 8, pp. 209212–209223, 2020.

[8] F. Zheng, W. Wu, B. Chen, and E. Koutroulis, "An optimized parameter design method for passivity-based control in a LCL-filtered grid-connected inverter," *IEEE Access*, vol. 8, pp. 189878–189890, 2020.

[9] R. Zhao, C. Wang, Q. Yan, H. Xu, and F. Blaabjerg, "Common-mode resonance damping and DC voltage balancing strategy for LCCL-filtered three-level photovoltaic grid-tied inverters," *IEEE Access*, vol. 8, pp. 13228–13239, 2020.

[10] S. Albatran, A. Koran, I. A. Smadi, and H. J. Ahmad, "Optimal design of passive RC-damped LCL filter for grid-connected voltage source inverters," *Electr. Eng.*, vol. 100, no. 4, pp. 2499–2508, Jul. 2018.

[11] S. Albatran, I. Smadi, H. Ahmad, and A. Koran, "Online optimal switching frequency selection for grid-connected voltage source inverters," *Electronics*, vol. 6, no. 4, p. 110, Dec. 2017.

[12] N. Mukherjee and D. De, "Analysis and improvement of performance in LCL filter-based PWM rectifier/inverter application using hybrid damping approach," *IET Power Electron.*, vol. 6, no. 2, pp. 309–325, Feb. 2013.

[13] S. A. Kharitonov, M. A. Petrov, D. V. Korobkov, M. A. Maslov, and T. Y. Zhoraev, "A principle of calculation dynamic and static power losses with hard-switching IGBT," in *Proc. 6th Annual. Int. Siberian Workshop Tuts. Electron Devices Mater.*, Jul. 2005, pp. 147–149.

[14] Y. Wu, M. A. Shafi, A. M. Knight, and R. A. Mcmahon, "Comparison of the effects of continuous and discontinuous PWM schemes on power losses of voltage-sourced inverters for induction motor drives," *IEEE Trans. Power Electron.*, vol. 26, no. 1, pp. 182–191, Jan. 2011.

[15] E. Un and A. M. Hava, "A near-state PWM method with reduced switching losses and reduced common-mode voltage for three-phase voltage source inverters," *IEEE Trans. Ind. Appl.*, vol. 45, no. 2, pp. 782–793, Mar. 2009.

[16] D. Zhao, V. S. S. P. K. Hari, G. Narayanan, and R. Ayyanar, "Space-vector-based hybrid pulsewidth modulation techniques for reduced harmonic distortion and switching loss," *IEEE Trans. Power Electron.*, vol. 25, no. 3, pp. 760–774, Mar. 2010.

[17] O. Oñederra, I. Kortabarria, I. M. de Alegría, J. Andreu, and J. I. Gárate, "Three-phase VSI optimal switching loss reduction using variable switching frequency," *IEEE Trans. Power Electron.*, vol. 32, no. 8, pp. 6570–6576, Aug. 2017.

[18] M. R. Ruman, D. Paul, A. Barua, A. K. Sarker, A. Iqbal, and S. Barua, "Design and implementation of SPWM inverter," in *Proc. Int. Conf. Comput., Commun., Intell. Syst. (ICCCIS)*, Oct. 2019, pp. 490–494.

[19] J. Muhlethaler, J. Biela, J. W. Kolar, and A. Ecklebe, "Improved core-loss calculation for magnetic components employed in power electronic systems," *IEEE Trans. Power Electron.*, vol. 27, no. 2, pp. 964–973, Feb. 2012.

[20] J. Muhlethaler, J. Biela, J. W. Kolar, and A. Ecklebe, "Core losseses under the DC bias condition based on steinmetz parameters," *IEEE Trans. Power Electron.*, vol. 27, no. 2, pp. 953–963, Feb. 2012.

[21] J. Reinert, A. Brockmeyer, and R. W. A. A. De Doncker, "Calculation of losses in ferro- and ferrimagnetic materials based on the modified Steinmetz equation," *IEEE Trans. Ind. Appl.*, vol. 37, no. 4, pp. 1055–1061, Jul. 2001.
[22] J. Li, T. Abdallah, and C. R. Sullivan, "Improved calculation of core losses with non-sinusoidal waveforms," in *Proc. 36th IAS Annu. Meeting*, Chicago, IL, USA, Sep. 2001, pp. 2203–2210.
[23] S. Yue, Y. Li, Q. Yang, X. Yu, and C. Zhang, "Comparative analysis of core losses calculation methods for magnetic materials under non-sinusoidal excitations," in *IEEE Trans. Magn.*, vol. 54, no. 11, pp. 1–5, Nov. 2018.
[24] M. Bartoli, N. Noferi, A. Reatti, and M. K. Kazimierczuk, "Modelling winding losses in high-frequency power inductors," *J. Circuits, Syst. Comput.*, vol. 5, no. 4, pp. 607–626, Dec. 1995.
[25] M. Bartoli, N. Noferi, A. Reatti, and M. K. Kazimierczuk, "Modeling Litz-wire winding losses in high-frequency power inductors," in *Proc. PESC Rec. 27th Annu. IEEE Power Electron. Spec. Conf.*, Jun. 1996, pp. 1690–1696.
[26] X. Nan and C. R. Sullivan, "Simplified high-accuracy calculation of eddy-current loss in round-wire windings," in *Proc. IEEE 35th Annu. Power Electron. Spec. Conf.*, Jun. 2004, pp. 873–879.
[27] B. Carsten, "High-frequency conductor losses in switch mode magnetics," in *Proc. HPFC*, 1986, pp. 155–176.
[28] J. A. Ferreira, "Improved analytical modeling of conductive losses in magnetic components," *IEEE Trans. Power Electron.*, vol. 9, no. 1, pp. 127–131, Jan. 1994.
[29] E. Bennett and S. C. Larson, "Effective resistance to alternating currents of multilayer windings," *Elect. Eng.*, vol. 59, no. 12, pp. 1010–1016, Dec. 1940.
[30] M. Vitelli, "Numerical evaluation of 2-D proximity effect conductor losses," *IEEE Trans. Power Del.*, vol. 19, no. 3, pp. 1291–1298, Jul. 2004.
[31] F. Casanellas, "Losses in PWM inverters using IGBTs," *IEE Proc.-Electr. Power Appl.*, vol. 141, no. 5, pp. 235–239, Sep. 1994.
[32] H. Jamal, S. Albatran, and I. A. Smadi, "Variable switching frequency algorithm for optimal tradeoff between switching losses and total demand distortion in grid-tied three-phase voltage-source inverters," in *Proc. IEEE Energy Convers. Congr. Expo. (ECCE)*, Sep. 2016, pp. 1–7.
[33] C. Kwang-Bo and L. Byang-Yoon. (Nov. 18, 1980). *Chang Sung Corporation*. Metal Powder Manufacturing Technology. Accessed: Oct. 8, 2020. [Online]. Available: http://www.changsung.com
[34] C. Sung, *Soft Magnetic Powder Cores*, document CO-180425 datasheet, 2018.
[35] R. V. Rao, "Teaching-learning-based optimization algorithm," *Teaching Learning Based Optimization Algorithm*. Cham, Switzerland: Springer, 2015, doi: 10.1007/978-3-319-22732-0_2.
[36] R. V. Rao, V. J. Savsani, and D. P. Vakharia, "Teaching–learning-based optimization: An optimization method for continuous non-linear large scale problems," *Inf. Sci.*, vol. 183, no. 1, pp. 1–15, Jan. 2012.
[37] Z. Zhai, S. Li, Y. Liu, and Z. Li, "Teaching-learning-based optimization with a fuzzy grouping learning strategy for global numerical optimization," *J. Intell. Fuzzy Syst.*, vol. 29, no. 6, pp. 2345–2356, Nov. 2015.
[38] A. Koran, S. Albatran, and J.-S. Lai, "Analytical factorized model for stability analysis and optimization of shunt RC damped LCL filter for grid-connected voltage source inverters," *IEEE Trans. Power Electron.*, vol. 35, no. 7, pp. 6830–6841, Jul. 2020.
[39] *IEEE Recommended Practices and Requirements for Harmonic Control in Electrical Power Systems*, Standard IEEE 519, 1992.
[40] K. Arulkumar, D. Vijayakumar, and K. Palanisamy, "Design of optimal LLCL filter with an improved control strategy for single phase grid connected PV inverter," *Int. J. Power Electron. Drive Syst. (IJPEDS)*, vol. 9, no. 1, p. 114, Mar. 2018.
[41] R. E. Smallman and R. J. Bishop, *Modern Physical Metallurgy and Materials Engineering*, 6th ed. Oxford, U.K.: Butterworth-Heinemann, 1999, pp. 168–196.
[42] R. E. Smallman and A. H. W. Ngan, "Physical Properties," in *Modern Physical Metallurgy*. Oxford, U.K.: Butterworth-Heinemann, 2014, pp. 317–356.
[43] *IEEE Recommended Practice and Requirements for Harmonic Control in Electric Power Systems*, Standard 519-2014 (Revision IEEE Std 519-1992), Jun. 2014, pp. 1–29.

AHMED KORAN (Member, IEEE) received the B.Sc. degree in electrical power engineering from Yarmouk University, Irbid, Jordan, in 2004, the M.Sc. degree in electrical engineering from the Illinois Institute of Technology (IIT), Chicago, USA, in 2007, and the Ph.D. degree from Virginia Polytechnic Institute and State University (VTech), Blacksburg, USA, in 2013.

Since 2013, he has been with the Department of Electrical Power Engineering, Yarmouk University, as an Associate Professor, and was appointed as the department chair, from 2014 to 2016. Currently, he is the Vice Dean of the Hijjawi Faculty for Engineering Technology, Yarmouk University. His teaching philosophy is to expand the limits of student's knowledge and their analytical abilities in the fields of power electronics and electric motor drives. His research interests include the modeling, design, and optimization of power electronics and motor drives systems and their applications in renewable energy and wireless power transfer.

SAHER ALBATRAN (Senior Member, IEEE) received the B.Sc. degree in electric power engineering from Yarmouk University, Irbid, Jordan, in 2005, the M.Sc. degree in electric power and control engineering from the Jordan University of Science and Technology, Irbid, and the Ph.D. degree in electrical engineering from Mississippi State University, MS, USA, in 2013.

He is currently an Associate Professor with the Jordan University of Science and Technology. His research interests include control of power electronics, pulse-width modulation, inverter topologies, power system operation, renewable energy, filter design, and control.

DOAA ALSHORMAN received the B.Sc. degree in electrical and electronic engineering from Mu'tah University, Alkarak, Jordan, in 2015, and the M.Sc. degree in electrical power engineering from Yarmouk University, Irbid, Jordan, in 2021.

Her research interests include the modeling, design, and optimization of power electronics systems.